A New Methodology for the Optimal Charging Coordination of Electric Vehicles Considering Vehicle-to-Grid Technology

Carlos Sabillón Antúnez, John F. Franco, *Member, IEEE*, Marcos J. Rider, *Member, IEEE*, and Ruben Romero, *Senior Member, IEEE*

***Abstract*—In this work, a new methodology based on a mixed integer linear programming formulation is proposed to solve the optimal charging coordination of electric vehicles (EVs) in unbalanced electrical distribution systems (EDS) considering vehicle-to-grid (V2G) technology. The steady-state operation of the EDS is represented using the real and imaginary parts of voltages and currents at nodes and circuits respectively. Distributed generation (DG) and the imbalance of the system circuits and loads are taken into account. The developed method defines an optimal charging schedule for the EVs. This charging schedule considers the EVs' arrival and departure times and their arrival state of charge, along with the energy contribution of EVs equipped with V2G technology. The presented formulation was tested in a 123-node distribution system. The charging schedule obtained was compared in terms of V2G and DG scenarios, demonstrating the efficiency of the proposed method.**

***Index Terms*—Charging coordination problem, electric vehicles, mixed integer linear programming, vehicle-to-grid.**

I. Nomenclature

The notation used throughout this paper is reproduced below for quick reference.

Sets:

F	sets of phases, {A,B,C}
L	sets of circuits
N	sets of nodes
Ξ	sets of electric vehicles
$V2G$	sets of vehicles-to-grid
T	sets of time intervals

Constants:

$\alpha^{G}_{n,t}$	energy cost at node n in time interval t
β	electric vehicle energy curtailment cost
$\gamma\left(u,m,f\right)$	function that indicates whether electric vehicle u is connected at node m and phase f
Δ_t	duration of the time interval t
ϕ_n	minimum power factor for the operation of the distributed generator at node n
$\overline{\delta}_{mn}$	discretization step for the current of circuit mn
$\overline{\lambda}$	number of blocks of the square current piecewise linearization
θ	vector of reference phase angles
θ_1	maximum negative deviation of the phase angle from the reference angle for each phase
θ_2	maximum positive deviation of the phase angle around the reference angle for each phase
$\sigma_{mn,\lambda}$	slope of the λth block of the piecewise linearization for the current of circuit mn
ξ	minimum percentage of energy for electric vehicles
$B_{mn,f}$	shunt susceptance of circuit mn for phase f
$\overline{E}^{EV}_{u}$	energy capacity of electric vehicle u
E^{ini}_{u}	initial charge state of electric vehicle u
$\overline{I}_{mn}$	maximum current flow magnitude of circuit mn
$P^{D}_{n,f,t}$	active power demand at node n for phase f in time interval t
$\overline{P}^{CH}_{u}$	maximum power consumption of electric vehicle u
$\overline{P}^{DC}_{u}$	maximum power injection of electric vehicle u
$\overline{P}^{G}_{n}$	maximum active power of the distributed generator at node n
$Q^{D}_{n,f,t}$	reactive power demand at node n for phase f in time interval t
$\overline{Q}^{G}_{n},\underline{Q}^{G}_{n}$	maximum and minimum reactive powers of the distributed generator at node n
$R_{mn,f,h}$	resistance of circuit mn between phases f and h
S	substation node
T_f	last time interval of the time period
$\overline{V},\underline{V}$	maximum and minimum voltage magnitude limits
$V^{re^*}_{n,f,t}$	real part of the estimated voltage at node n for phase f in time interval t
$V^{im^*}_{n,f,t}$	imaginary part of the estimated voltage at node n for phase f in time interval t
$\widehat{V}^{re*}_{u,t}$	real part of the estimated voltage at the node and phase associated with electric vehicle u in time interval t

Manuscript received July 07, 2015; revised October 28, 2015; accepted December 01, 2015. Date of publication January 01, 2016; date of current version March 18, 2016. This work was supported by the Brazilian institutions CAPES, CNPq, FAPESP and CPFL. Paper no. TSTE-00571-2015.

C. Sabillón Antúnez, J. F. Franco and R. Romero are with the Departamento de Engenharia Elétrica, Faculdade de Engenharia de Ilha Solteira, Universidade Estadual Paulista (UNESP), 15385-000 Ilha Solteira, São Paulo, Brazil (e-mail: cfsa27@gmail.com; jffranco@gmail.com; ruben@dee.feis.unesp.br).

M. J. Rider is with the Department of Systems and Energy, School of Electrical and Computer Engineering University of Campinas (UNICAMP), 13083-852 Campinas, Brazil (e-mail: mjrider@dsee.fee.unicamp.br).

Color versions of one or more of the figures in this paper are available online at http://ieeexplore.ieee.org.

Digital Object Identifier 10.1109/TSTE.2015.2505502

$\widehat{V}^{im*}_{u,t}$ imaginary part of the estimated voltage at the node and phase associated with electric vehicle u in time interval t

$X_{mn,f,h}$ reactance of circuit mn between phases f and h

Variables:

$\delta_{mn,f,t,\lambda}$ value of the λth block of the piecewise linearization for the current of circuit mn for phase$f$ in time interval t

τ_u time interval at which charge and discharge cycles are separated for electric vehicle u

$\dot{\tau}_u$ auxiliary variable used for the calculation of τ_u

$E^{EV}_{u,t}$ energy of electric vehicle at node u at the end of time interval t

$E^{EV}_{u,T}$ energy of electric vehicle at node u at the end of the time period

E^{SH}_{u} energy curtailment of electric vehicle u at the end of the time period

$I^{Dim}_{n,f,t}$ imaginary part of the current demanded by a conventional load at node n for phase f in time interval t

$I^{Dre}_{n,f,t}$ real part of the current demanded by a conventional load at node n for phase f in time interval t

$I^{EVim}_{u,t}$ imaginary part of the current demanded by electric vehicle u in time interval t

$I^{EVre}_{u,t}$ real part of the current demanded by electric vehicle u in time interval t

$I^{Gim}_{n,f,t}$ imaginary part of the current generated at node n for phase f in time interval t

$I^{Gre}_{n,f,t}$ real part of the current generated at node n for phase f in time interval t

$I^{im}_{mn,f,t}$ imaginary part of the current in circuit mn for phase f in time interval t

$I^{im+}_{mn,f,t}$ positive component of the current's imaginary part in circuit mn for phase f in time interval t

$I^{im-}_{mn,f,t}$ negative component of the current's imaginary part in circuit mn for phase f in time interval t

$I^{re}_{mn,f,t}$ real part of the current in circuit mn for phase f in time interval t

$I^{re+}_{mn,f,t}$ positive component of the current's real part in circuit mn for phase f in time interval t

$I^{re-}_{mn,f,t}$ negative component of the current's real part in circuit mn for phase f in time interval t

$I^{sqr}_{mn,f,t}$ square of the current in circuit mn for phase f in time interval t

$P^{EV}_{u,t}$ active power consumption of electric vehicle u in time interval t

$P^{G}_{n,t}$ active power generated at node n in time interval t

$Q^{G}_{n,t}$ reactive power generated at node n in time interval t

$V^{re}_{n,f,t}$ real part of the voltage at node n for phase$f$ in time interval t

$V^{im}_{n,f,t}$ imaginary part of the voltage at node n for phase f in time interval t

$\widehat{V}^{re}_{u,t}$ real part of the voltage at the node and phase associated with electric vehicle u in time interval t

$\widehat{V}^{im}_{u,t}$ imaginary part of the voltage at the node and phase associated with electric vehicle u in time interval t

$y_{u,t}$ binary variable associated with the charging state of electric vehicle u in time interval t

$z_{u,t}$ binary variable associated with the discharging state of V2G vehicle u in time interval t

II. Introduction

In RECENT years, energy and transport sectors have been experiencing revolutionary changes due to environmental concerns and desires for energy independence. The transport sector is becoming part of the electrification movement. As such, the use of electric vehicles (EV) will increase over the coming years [1], [2]. Instead of fossil fuel energy, EVs use batteries to store the energy needed for transportation. Reducing the dependency on fossil fuel, these batteries are charged on an electric distribution system (EDS). If the charging of EVs is not controlled, the EDS can experience overloads, voltage limit violations, and an excessive increase in power losses [3], [4]. Given the increasing presence of EVs in the EDS, these issues must be anticipated. To counteract the problem associated with a high load of EVs linked to the system, a charging schedule must be set to coordinate the recharging of EV batteries. The communication infrastructure of forthcoming smart grids will become an essential part of controlling EV recharging in EDSs [5].

The EV charging coordination (EVCC) problem seeks an optimal charging schedule for the recharging of EV batteries in a specific time period. In addition to throttling the battery charge, the optimal charging schedule must maximize the energy charged to the EV batteries and minimize power losses. Also, an economical operation for the EDS must be defined, while satisfying operational constraints. Various works have approached the EVCC problem in EDSs [4]–[6]. Charging costs are optimized in [6] by using a mixed integer linear programming (MILP) formulation in which battery charging profiles are detailed. Mobility demands and maximum power limits are considered, but the impact of the EV load on the grid is disregarded.

Real-time solutions for EVCC are presented in [7]–[9]. A multi-period optimization for EV charging in EDSs is proposed on [7]. This optimization aims to minimize the cost of charging EVs, while disregarding the energy cost of the loads on the EDS. A nonlinear programming model is proposed and solved using a nonlinear programming function of MATLAB. In [8], the goal is to optimally charge the EVs and minimize system operating costs without violating the power system constraints. A prediction unit that forecasts the EV power demand is proposed to ensure the feasibility of the charging process. A two-stage optimization process is presented to ensure effective charging coordination. In [9], an algorithm based on sensitivities is proposed for the real-time coordination of EV charging considering the random arrivals and departures of EVs, voltage

profile, and power generation limits, in order to minimize the total energy cost.

In [10]–[12], EV charging management models with operational frameworks based on multi-agent system (MAS) technology are proposed. A distributed price-based control method that considers owners' preferences is developed in [10]. In [11], a charging control method developed over a three-layer architecture MAS is presented. The optimal EV charging schedule at the beginning of each charging period is obtained by solving an optimization problem, which considers individual EV needs. The charging schedules are later validated to ensure the technical viability of the solution. In [12], important features are added to the approach presented in [11]. The control method presented in [12] is also based on a three-layer MAS. This formulation presents not only an optimal charging scheme for normal operation but also an emergency planning method employed when normal conditions are restored after a technical limit breach. However, the EVs are disconnected to restore the proper performance of the EDS (i.e., thermal or voltage limits are already unfulfilled) and not to avoid technical limit violations.

As EVs are gaining relevance in EDSs, the idea of power flowing in both directions is taking hold. The ability of EVs to inject power into the grid is called vehicle-to-grid (V2G) technology. V2G can be defined as the purveyance of energy and ancillary services from an EV to the grid [13]. Either at home or in a parking lot, EVs with V2G technology (EV-V2Gs) can provide power to the grid, increasing the stability and reliability of the EDS and reducing costs [14]. Studies of battery sizing together with economic assessments of V2G availability have proved how profitable this technology may become [15], [16].

Different approaches to taking advantage of V2G technology have been proposed in the specialized literature. In [17], an aggregator for V2G frequency regulation is developed. This approach establishes that any vehicle that is idle and under aggregator control is a potential provider of a regulation service, considering its available power capacity. The objective is to optimize the aggregator's revenue, while fulfilling the energy requirements of the EV owner. An estimation algorithm for V2G real-time capacity is presented in [18]. This paper proposes a dynamic scheduling algorithm for EV charging in high-rise residential buildings, office buildings, and commercial buildings. Furthermore, the capacity of an EV fleet to supply V2G power to a building during peak hours is demonstrated, and renewable energy resources are taken into account. The EV-V2Gs were shown to be effective for load peak shaving, but the impact on the EV battery's lifetime was not assessed.

Recent works such as [18] and [19] have foregrounded the importance of the dynamic scheduling on EV charging. In the latter work, the issues arising in the EDS due to uncontrolled EV charging processes are remarked. Nevertheless, the EV charging scheduling alone does not account for EV owners' behavior patterns or unforeseen changes in EV features. Dynamic scheduling is, therefore, crucial for attending EV owners' needs because scheduling may involve the random arrivals and departures of EVs and varying values for the initial charge of the EV batteries. These are the most important EV characteristics addressed by the EVCC problem, and the correct inclusion of these features ensures the better performance of the presented solution method.

A step-by-step methodology based on a MILP formulation is proposed in this paper to solve the optimal charging coordination of EVs in unbalanced EDSs considering V2G technology. The steady-state operation of the EDS is represented using the real and imaginary parts of voltages and currents at nodes and circuits, respectively. Linearization techniques were applied to the formulation in order to obtain a MILP model. The imbalance of the system circuits and loads are taken into account. In addition, the proposed formulation considers distributed generation (DG). The developed method defines an optimal charging schedule for the EVs considering the EVs' arrival and departure times and their arrival state of charge, along with the energy contribution of EVs equipped with V2G technology. The model was written in mathematical modeling language AMPL and solved using the commercial solver CPLEX. The classical optimization techniques used to solve the MILP formulation guarantee the optimal solution to the problem. The presented formulation was tested in a 123-node distribution system. The charging schedules obtained for different EV load scenarios evaluated on the EDS prove the robustness of the methodology.

This work's main contributions are as follows:

- A new methodology for dynamically controlling the EVCC problem considering V2G technology in unbalanced distribution systems. The methodology is based on an MILP formulation that offers the optimal solution to the problem;
- A step-by-step methodology that considers the randomness of EVs' arrivals and departures times and initial state of charge, as well as different battery sizes and forecast uncertainties;
- A methodology that enhances the EDS operation by including unforeseen EV loads at any time interval. This approach not only solves the EVCC problem, but also optimizes the operation of the EDS, reducing the overall energy costs, while satisfying operational constraints such as voltage and thermal limits.

III. Methodology

The presented methodology solves the EVCC problem finding an optimal schedule for the energy exchange between EV batteries and the grid; moreover, an economic operation for the EDS is defined and operational constraints are satisfied. The optimal charging schedule must minimize the energy cost, avoiding curtailment on the EV batteries and reducing power losses in the EDS. As V2G technology on EVs is taken into account, the solution must provide an optimal schedule that determines when the EV batteries must be charged and when the EV-V2Gs must inject energy into the grid. The complexity of the charging schedule increases, as it is responsible for throttling the battery charge and for allowing the grid to use the vehicles' battery stored energy. In this work, the following considerations are assumed:

- At departure, the vehicles should be completely charged.
- The initial state of charge (SOC) of every vehicle is known when the vehicle is plugged into the grid.

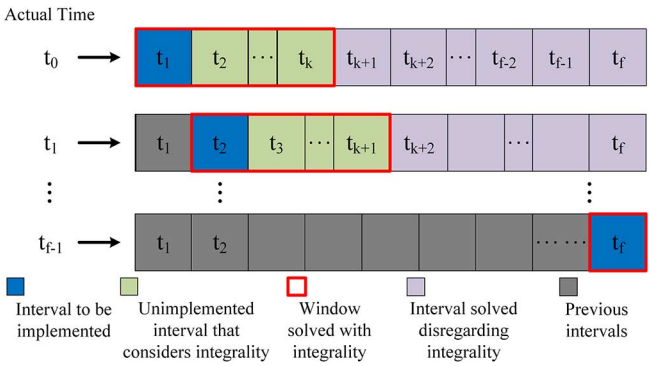

Fig. 1. Solution cycle.

- The batteries can be controlled in each time interval into which the time period is divided.
- The EV-V2Gs can be controlled in order to inject power into the grid according to their available energy.
- The EV-V2Gs owners permit the EDS operator to utilize the energy stored in their vehicles.

Operational constraints such as voltage limits, active and reactive power generation limits, and maximum currents limits, must be satisfied by the model as the charging schedule is being optimized. When being plugged in, the EV's SOC is read, and the EV user may provide a departure time; otherwise, it will be assumed that the vehicle will remain plugged in until a probable time interval has lapsed, as determined by an EV record of departure. The model is solved in every time interval updating the actual number of connected EVs to be charged. Fig. 1 shows how the model is solved for each time interval defining the next step to be implemented by the EDS operator. The red boxes in Fig. 1 indicate how the binary nature of variables $y_{n,t}$ and $z_{n,t}$, associated with the charging and discharging of the EVs, is considered only for the next $k-$intervals (defined by the EDS operator); in the remaining time intervals, the binary nature of those variables is disregarded.

The EVs' charging schedule will be generated between arrival and departure, ideally dispatching a fully charged battery for every vehicle. Energy curtailment on any EV at departure will incur a penalty. With the model being solved in every time interval, the charging schedule is to be constructed step-by-step, with previous $y_{n,t}$ and $z_{n,t}$ values given from preceding solutions and only the immediate interval's $y_{n,t}$ and $z_{n,t}$ values fixed. When defining the charging schedule, the later connection of EVs is taken into account in order to avoid overloads in the system when added to the EVs already connected. Therefore, the proposed model includes expected arrival times in the solution. Possible plugs, estimated arrival times, and SOCs are used to get more accurate charging schedules for initial solutions. Later on in the process, when the EVs are actually plugged in, the information can be updated with the real parameters. In cases where the possible arrival time is reached and the EV has not arrived, a different estimation may be used, or the EV may be disregarded altogether. Several techniques can be applied to EVs in order to obtain the estimated parameters for initial SOCs, arrival times and departure times, such as those in [20]–[22]. The mathematical model takes into account these parameters when building a charging schedule for every vehicle between their arrival and departure times.

IV. Mathematical Programming Model for the EV Charging Coordination Problem

A mixed integer nonlinear programming (MINLP) model is presented in (1)–(23) to solve the EVCC problem considering EVs and EV-V2Gs. The EVCC problem is later modeled as a mixed-integer linear programming (MILP) problem. This will improve the solution's robustness and permit the utilization of classical optimization techniques and commercial software, which will guarantee the optimal solution to the problem. In order to obtain a MILP for the EVCC problem, linearization techniques are applied to the MINLP nonlinear expressions.

The circuits and the conventional loads are considered using a three-phase representation, as the EDS is modeled as an unbalanced system. The steady state operation of an unbalanced EDS is indicated by the set of equations (2)–(14), based on the model presented in [23], which considers the presence of DG. In this work, active and reactive power injections of DGs are taken into account and the loads are modeled as a constant power type. EVs may arrive and leave in any time interval within the charging period. If no departure time is specified, the model will schedule a fully charged battery by the EV's probable departure time interval. In effect, before its departure time, a vehicle may have any charge level between its initial SOC and its $\overline{E}_u^{EV}$. For EV-V2Gs, this energy level may be lower than its initial SOC but not greater than the maximum depth of discharge (DoD), maintaining at least an minimum energy level $\left(\bar{E}_u^{EV}\xi\right)$. The time period is divided into several time intervals ordered in the set T; the time interval that begins at a specific time t is associated with the t element from set T. The time duration for every time interval is represented by Δ_t. The proposed model is solved at the beginning of each time interval, constructing a step-by-step solution over the entire time period, and updating the number of EVs connected and their associated data. The objective function of the EVCC problem represented by (1) aims to minimize the cost of the energy provided by the substation and the distributed generators (the first and second terms, respectively) and to reduce the EV's energy curtailment if the EVs can not be completely charged (third term).

$$\min \sum_{f\in F}\sum_{t\in T}\alpha_{S,t}^{G}\Delta_t\left(V_{S,f,t}^{re}I_{S,f,t}^{Gre}+V_{S,f,t}^{im}I_{S,f,t}^{Gim}\right) + \sum_{n\in N}\sum_{t\in T}\alpha_{n,t}^{G}\Delta_t P_{n,t}^{G}+\sum_{u\in\Xi}\beta E_u^{SH} \tag{1}$$

Subject to:

$$I_{m,f,t}^{Gre}+\sum_{km\in L}I_{km,f,t}^{re}-\sum_{mn\in L}I_{mn,t}^{re} -\left(\sum_{km\in L}B_{km,f}+\sum_{mn\in L}B_{mn,f}\right)\frac{V_{m,f,t}^{im}}{2}=I_{m,f,t}^{Dre} +\sum_{u\in\Xi}I_{u,t}^{EVre}\gamma(u,m,f)\qquad\forall m\in N, f\in F, t\in T \tag{2}$$

$$I^{Gim}_{m,f,t} + \sum_{km\in L} I^{im}_{km,f,t} - \sum_{mn\in L} I^{im}_{mn,t} - \left(\sum_{km\in L} B_{km,f} + \sum_{mn\in L} B_{mn,f}\right)\frac{V^{re}_{m,f,t}}{2} = I^{Dim}_{m,f,t} + \sum_{u\in\Xi} I^{EVim}_{u,t}\gamma(u,m,f) \quad \forall m\in N, f\in F, t\in T \quad (3)$$

$$P^{D}_{n,f,t} = V^{re}_{n,f,t} I^{Dre}_{n,f,t} + V^{im}_{n,f,t} I^{Dim}_{n,f,t} \quad \forall n\in N, f\in F, t\in T \quad (4)$$

$$Q^{D}_{n,f,t} = -V^{re}_{n,f,t} I^{Dim}_{n,f,t} + V^{im}_{n,f,t} I^{Dre}_{n,f,t}, \forall n\in N, f\in F, t\in T \quad (5)$$

$$V^{re}_{m,f,t} - V^{re}_{n,f,t} = \sum_{h\in F}(R_{mn,f,h} I^{re}_{mn,h,t} - X_{mn,f,h} I^{im}_{mn,h,t}) \quad \forall mn\in L, f\in F, t\in T \quad (6)$$

$$V^{im}_{m,f,t} - V^{im}_{n,f,t} = \sum_{h\in F}(X_{mn,f,h} I^{re}_{mn,h,t} + R_{mn,f,h} I^{im}_{mn,h,t}) \quad \forall mn\in L, f\in F, t\in T \quad (7)$$

$$0 \le P^{G}_{n,t} \le \overline{P}^{G}_{n} \quad \forall n\in N, t\in T \quad (8)$$

$$\underline{Q}^{G}_{n} \le Q^{G}_{n,t} \le \overline{Q}^{G}_{n} \quad \forall n\in N, t\in T \quad (9)$$

$$|Q^{G}_{n,t}| \le P^{G}_{n,t}\tan(\arccos(\phi_n)) \quad \forall n\in N, t\in T \quad (10)$$

$$\frac{P^{G}_{n,t}}{3} = V^{re}_{n,f,t} I^{Gre}_{n,f,t} + V^{im}_{n,f,t} I^{Gim}_{n,f,t} \quad \forall n\in N, f\in F, t\in T \quad (11)$$

$$\frac{Q^{G}_{n,t}}{3} = -V^{re}_{n,f,t} I^{Gim}_{n,f,t} + V^{im}_{n,f,t} I^{Gre}_{n,f,t}, \ \forall n\in N, f\in F, t\in T \quad (12)$$

$$\underline{V}^2 \le {V^{re}_{n,f,t}}^2 + {V^{im}_{n,f,t}}^2 \le \overline{V}^2 \quad \forall n\in N, f\in F, t\in T \quad (13)$$

$$0 \le {I^{re}_{mn,f,t}}^2 + {I^{im}_{mn,f,t}}^2 \le {\overline{I}_{mn}}^2 \quad \forall mn\in L, f\in F, t\in T \quad (14)$$

$$P^{EV}_{u,t} = V^{re}_{u,t} I^{EVre}_{u,t} + V^{im}_{u,t} I^{EVim}_{u,t} \quad \forall u\in\Xi, t\in T \quad (15)$$

$$0 = -V^{re}_{u,t} I^{EVim}_{u,t} + V^{im}_{u,t} I^{EVre}_{u,t} \quad \forall u\in\Xi, t\in T \quad (16)$$

$$\bar{E}^{EV}_{u} = E^{EV}_{u,T} + E^{SH}_{u} \quad \forall u\in\Xi \quad (17)$$

$$P^{EV}_{u,t} = \bar{P}^{CH}_{u} y_{u,t} - \bar{P}^{DC}_{u} z_{u,t} \quad \forall u\in\Xi, t\in T \quad (18)$$

$$E^{EV}_{u,t} = E^{ini}_{u} + \sum_{k\in T, k\le t} \Delta_k P^{EV}_{u,k} \quad \forall u\in\Xi, t\in T \quad (19)$$

$$\min\left(E^{ini}_{u}, \bar{E}^{EV}_{u}\xi\right) \le E^{EV}_{u,t} \le \bar{E}^{EV}_{u} \quad \forall u\in\Xi, t\in T \quad (20)$$

$$y_{u,t} + z_{u,t} \le 1 \quad \forall\, u\in\Xi, t\in T \quad (21)$$

$$z_{u,t} \in \{0,1\} \quad \forall u\in\Xi, t\in T \quad (22)$$

$$y_{u,t} \in \{0,1\} \quad \forall u\in\Xi, t\in T \quad (23)$$

Equations (2) and (3) represent the balance of the real and imaginary parts of the circuit currents at each node, respectively. The term $\gamma(u,m,f)$ is a binary function that takes a value of 1 if the EV u is connected at node m and at phase f. Equations (4) and (5) define the load currents. The relationship between power, voltage, and current for the loads may also be written as shown in (24) and (25).

$$I^{Dre}_{n,f,t} = \frac{P^{D}_{n,f,t} V^{re}_{n,f,t} + Q^{D}_{n,f,t} V^{im}_{n,f,t}}{{V^{re}_{n,f,t}}^2 + {V^{im}_{n,f,t}}^2}, \ \forall n\in N, f\in F, t\in T \quad (24)$$

$$I^{Dim}_{n,f,t} = \frac{P^{D}_{n,f,t} V^{im}_{n,f,t} - Q^{D}_{n,f,t} V^{re}_{n,f,t}}{{V^{re}_{n,f,t}}^2 + {V^{im}_{n,f,t}}^2}, \ \forall n\in N, f\in F, t\in T \quad (25)$$

If the right part of (24) and (25), which are nonlinear functions of the voltage's real and imaginary parts, are represented by $g(P^{D}_{n,f,t}, Q^{D}_{n,f,t}, V^{re}_{n,f,t}, V^{im}_{n,f,t})$ and $h(P^{D}_{n,f,t}, Q^{D}_{n,f,t}, V^{re}_{n,f,t}, V^{im}_{n,f,t})$, respectively, and taking advantage of the relatively small and limited variation range of the voltage magnitude in an EDS, these equations can be linearized around an estimated operation point $(V^{re^*}_{n,f,t}, V^{im^*}_{n,f,t})$, as shown in (26) and (27).

$$I^{Dre}_{n,f,t} = g^* + \left.\frac{\partial g}{\partial V^{re}}\right|^* (V^{re}_{n,f,t} - V^{re^*}_{n,f,t}) + \left.\frac{\partial g}{\partial V^{im}}\right|^* (V^{im}_{n,f,t} - V^{im^*}_{n,f,t}) \quad \forall n\in N, f\in F, t\in T \quad (26)$$

$$I^{Dim}_{n,f,t} = h^* + \left.\frac{\partial h}{\partial V^{re}}\right|^* (V^{re}_{n,f,t} - V^{re^*}_{n,f,t}) + \left.\frac{\partial h}{\partial V^{im}}\right|^* (V^{im}_{n,f,t} - V^{im^*}_{n,f,t}) \quad \forall n\in N, f\in F, t\in T \quad (27)$$

Linear equations (26) and (27) can be used to approximate the currents demanded by the loads previously represented by the nonlinear expressions (4) and (5). The quality of the estimated operation point will define the approximation error. Historical data and the knowledge of the EDS operator are used to estimate the operation point. Equations (6) and (7) are the result of applying Kirchhoff's Voltage Law to each independent loop in the EDS. Constraints (8)–(10) define the operation limits of the DGs and (11)–(12) represent their active and reactive powers. The nonlinearity of the DGs active and reactive powers is approximated using an estimated operation point $(V^{re^*}_{n,f,t}, V^{im^*}_{n,f,t})$ as shown in (28)–(29).

$$\frac{P^{G}_{n,t}}{3} = V^{re^*}_{n,f,t} I^{Gre}_{n,f,t} + V^{im^*}_{n,f,t} I^{Gim}_{n,f,t} \quad \forall n\in N, f\in F, t\in T \quad (28)$$

$$\frac{Q^{G}_{n,t}}{3} = -V^{re^*}_{n,f,t} I^{Gim}_{n,f,t} + V^{im^*}_{n,f,t} I^{Gre}_{n,f,t}, \quad \forall n\in N, f\in F, t\in T \quad (29)$$

The limits for the voltage magnitude in each circuit are stated in (13). The phase angle variation around the reference voltage for each phase in the EDS is small. Because of this fact, (13) can be modeled by defining the boundaries of the feasible region of the voltage, considering operation limits. If θ_1 and θ_2

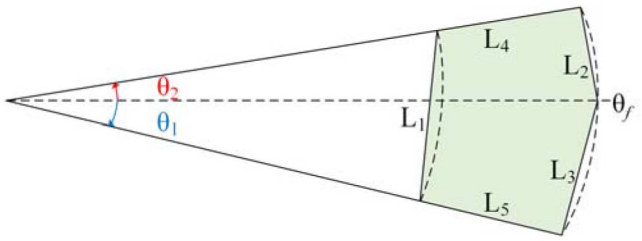

Fig. 2. Constraints for voltage limits (phase A).

are the maximum negative and maximum positive deviations of the phase angle around the reference ($\theta = [0°, +120°, -120°]$) for each phase, then (30), (31), (32), (33), and (34) limit the voltage magnitudes between $[\underline{V}, \overline{V}]$ and the phase angles $[\theta_f - \theta_1, \theta_f + \theta_2]$. Constraints (30), (31), (32), (33), and (34) are related with lines L_1, L_2, L_3, L_4 and L_5, respectively, as shown in Fig. 2.

$$V^{im}_{n,f,t} \le \frac{\sin(\theta_f+\theta_2)-\sin(\theta_f-\theta_1)}{\cos(\theta_f+\theta_2)-\cos(\theta_f-\theta_1)} \left[V^{re}_{n,f,t} - \underline{V}\cos(\theta_f+\theta_2)\right] + \underline{V}\sin(\theta_f+\theta_2) \quad \forall n \in N, f = A, t \in T \quad (30)$$

$$V^{im}_{n,f,t} \le \frac{\sin(\theta_f+\theta_2)-\sin\theta_f}{\cos(\theta_f+\theta_2)-\cos\theta_f} \left[V^{re}_{n,f,t} - \overline{V}\cos\theta_f\right] + \overline{V}\sin\theta_f \quad \forall n \in N, f = A, t \in T \quad (31)$$

$$V^{im}_{n,f,t} \ge \frac{\sin(\theta_f-\theta_1)-\sin\theta_f}{\cos(\theta_f-\theta_1)-\cos\theta_f} \left[V^{re}_{n,f,t} - \overline{V}\cos\theta_f\right] + \overline{V}\sin\theta_f \quad \forall n \in N, f = A, t \in T \quad (32)$$

$$V^{im}_{n,f,t} \le V^{re}_{n,f,t}\tan(\theta_f+\theta_2) \quad \forall n \in N, f = A, t \in T \quad (33)$$

$$V^{im}_{n,f,t} \ge V^{re}_{n,f,t}\tan(\theta_f-\theta_1) \quad \forall n \in N, f = A, t \in T \quad (34)$$

The limits for current capacity in each circuit are stated in (14). As shown in [24], (14) is linearized using (35)–(42). The terms $\sum_{\lambda=1}^{\overline{\lambda}} \sigma_{mn,\lambda}\delta^{re}_{mn,f,t,\lambda}$ and $\sum_{\lambda=1}^{\overline{\lambda}} \sigma_{mn,\lambda}\delta^{im}_{mn,f,t,\lambda}$ are the linear approximations of ${I^{re}_{mn,f,t}}^2$ and ${I^{im}_{mn,f,t}}^2$, respectively. $\sigma_{mn,\lambda}$ and $\overline{\delta}_{mn}$ are constant parameters, as defined by (43) and (44).

$$I^{sqr}_{mn,f,t} = \sum_{\lambda=1}^{\overline{\lambda}} \sigma_{mn,\lambda}\delta^{re}_{mn,f,t,\lambda} + \sum_{\lambda=1}^{\overline{\lambda}} \sigma_{mn,\lambda}\delta^{im}_{mn,f,t,\lambda} \quad \forall mn \in L, f \in F, t \in T \quad (35)$$

$$I^{re}_{mn,f,t} = I^{re+}_{mn,f,t} - I^{re-}_{mn,f,t} \quad \forall mn \in L, f \in F, t \in T \quad (36)$$

$$I^{im}_{mn,f,t} = I^{im+}_{mn,f,t} - I^{im-}_{mn,f,t} \quad \forall mn \in L, f \in F, t \in T \quad (37)$$

$$I^{re+}_{mn,f,t} + I^{re-}_{mn,f,t} = \sum_{\lambda=1}^{\overline{\lambda}} \delta^{re}_{mn,f,t,\lambda}, \quad \forall mn \in L, f \in F, t \in T \quad (38)$$

$$I^{im+}_{mn,f,t} + I^{im-}_{mn,f,t} = \sum_{\lambda=1}^{\overline{\lambda}} \delta^{im}_{mn,f,t,\lambda}, \quad \forall mn \in L, f \in F, t \in T \quad (39)$$

$$0 \le \delta^{re}_{mn,f,t,\lambda} \le \overline{\delta}_{mn}, \ \forall mn \in L, f \in F, t \in T, \lambda = 1 \ldots \overline{\lambda} \quad (40)$$

$$0 \le \delta^{im}_{mn,f,t,\lambda} \le \overline{\delta}_{mn}, \ \forall mn \in L, f \in F, t \in T, \lambda = 1 \ldots \overline{\lambda} \quad (41)$$

$$I^{re+}_{mn,f,t}, I^{re-}_{mn,f,t}, I^{im+}_{mn,f,t}, I^{im-}_{mn,f,t} \ge 0 \quad \forall mn \in L, f \in F, t \in T \quad (42)$$

$$\sigma_{mn,\lambda} = (2\lambda - 1)\overline{\delta}_{mn} \quad \forall mn \in L, \lambda = 1 \ldots \overline{\lambda} \quad (43)$$

$$\overline{\delta}_{mn} = \frac{\overline{I}_{mn}}{\overline{\lambda}} \quad \forall mn \in L \quad (44)$$

Along with the estimated operation point, the number of discretization blocks $\overline{\lambda}$ must be adjusted in order to enhance the quality of the linear approximations. The EVs' active and reactive demanded powers are specified in (15) and (16). Similar to (11)–(12), (15)–(16) are approximated using $(V^{re^*}_{u,t}, V^{im^*}_{u,t})$; (45)–(46) show these approximations.

$$P^{EV}_{u,t} = V^{re^*}_{u,t} I^{EVre}_{u,t} + V^{im^*}_{u,t} I^{EVim}_{u,t} \quad \forall u \in \Xi, t \in T \quad (45)$$

$$0 = -V^{re^*}_{u,t} I^{EVim}_{u,t} + V^{im^*}_{u,t} I^{EVre}_{u,t} \quad \forall u \in \Xi, t \in T \quad (46)$$

Equation (17) establishes the energy balance between the EV's storage capacity, charged energy, and energy curtailment. The demanded power for each vehicle in each time interval is specified by (18). Equation (19) represents the energy stored in every EV in each time interval. The energy limits of an EV are defined by (20), which ensures that the maximum energy level is not violated for all EVs. Furthermore, the grid will not take more than the available energy from the EV-V2G batteries, complying with a security level that limits the minimum energy level for each EV battery. The binary variables $y_{n,t}$ and $z_{u,t}$ define the EV's charging state, influencing the demanded power directly. Equation (21) limits the direction of the power flow in each time interval for every EV. The set of EV charging state variables has a binary nature, as detailed in (22) and (23). These two variables, model the energy transference between an EV battery and the grid. $y_{n,t}$ has a value of 1 if the battery is charging at its maximum power $\overline{P}^{CH}_n$ and a value of 0 if the battery is not charging; $z_{n,t}$ has a value of 1 if the battery is injecting energy into the grid at its maximum capacity $\overline{P}^{DC}_n$ and a value of 0 otherwise. In this way, the EVCC problem is modeled as a MINLP in (1)–(23), the complete MILP model for the EVCC problem is modeled by:

$$\min (1)$$

Subject to: (2)–(3), (6)–(10), (17)–(23), (26)–(42), (45)–(46)

$$0 \le I^{sqr}_{mn,f,t} \le {\overline{I}_{mn}}^2 \quad \forall mn \in L, f \in F, t \in T \quad (47)$$

A linear relaxation of the MILP model, where the binary nature of the decision variables is temporarily ignored, is initially solved in order to obtain a more accurate estimated operation point. To extend the lifetime of the EV batteries, equations are included to separate the charging and discharging cycles of EV-V2Gs. Constraints (48)–(52) prevent alternation between charging and discharging cycles, thereby, disallowing

TABLE I
HOURLY ENERGY COST AND LOAD VARIATION

hour	energy cost $/kWh	% of peak load	hour	energy cost $/kWh	% of peak load
08:00	0.038	46	**20:00**	**0.075**	**91**
09:00	0.048	55	**21:00**	**0.077**	**87**
10:00	0.055	63	**22:00**	**0.07**	**75**
11:00	0.059	70	**23:00**	**0.06**	**65**
12:00	0.058	75	**00:00**	**0.048**	**55**
13:00	0.057	83	**01:00**	**0.036**	**40**
14:00	0.058	88	**02:00**	**0.034**	**37**
15:00	0.062	90	**03:00**	**0.03**	**35**
16:00	0.063	95	**04:00**	**0.028**	**33**
17:00	0.064	100	**05:00**	**0.027**	**33**
18:00	**0.066**	**100**	**06:00**	**0.027**	**41**
19:00	**0.07**	**93**	**07:00**	**0.029**	**44**

the commencement of a discharging cycle once the charging cycle has begun. In addition, these equations use the auxiliary variables $\dot{\tau}_{u,t}$ and τ_u to find the optimal time interval to switch from discharging to charging for every EV.

$$ty_{u,t} \geq \dot{\tau}_{u,t} \qquad \forall u \in V2G, t \in T \qquad (48)$$

$$tz_{u,t} \leq \tau_u \qquad \forall u \in V2G, t \in T \qquad (49)$$

$$1 \leq \tau_u \leq T_f \qquad \forall u \in V2G, t \in T \qquad (50)$$

$$\dot{\tau}_{u,t} \leq T_f y_{u,t} \qquad \forall u \in V2G, t \in T \qquad (51)$$

$$\tau_u - \dot{\tau}_{u,t} \leq T_f \left(1 - y_{u,t}\right) \qquad \forall u \in V2G, t \in T \qquad (52)$$

V. TESTS AND RESULTS

The proposed model was tested in a 123-node distribution system with nominal voltage of 4.16 kV based on [25]. The maximum and minimum voltage magnitude limits were 1.00pu and 0.90pu, respectively. The voltage magnitude at the substation was fixed at 1.0pu. The energy capacity of the EV batteries was 50 kWh for Tesla EVs and 20 kWh for Nissan Leafs [26], [27]. The charging maximum power was 10 kW and 4 kW, and for EV-V2Gs the discharging maximum power was 5 kW and 2 kW, respectively. The parameter $\overline{I}_{mn}$ was 500 A for all feeders. The time period was set from 18:00h to 08:00h, divided into half-hour time intervals; β was 10 US$/kWh. The parameters θ_1 and θ_2 were set to 5° and 3°, respectively, and $\overline{\lambda}$ was set at 10. The full day hourly energy cost and load variation percentage are presented in Table I. The considered time period is the bolded area on Table I and it is assumed that any vehicle can arrive and depart during this period.

Phases A, B, and C of the EDS were charged with 40.7%, 26.2%, and 33.1% of the total demand, respectively. The conventional demands of the system were 1420 kVA, 915 kVA and 1155 kVA, connected to phases A, B and C, respectively. Tests were carried out for nine different cases. Table II presents the different cases tested in the 123-node system and their specific features. For all cases, the k-number of time periods, which considers the binary nature of the charging variables, was set at 3. Table II also shows the dumb charge operation for Case I. In this instance, the EDS had the same settings as in Case I, except that the EV recharge was done without any charging coordination. This meant that the EV batteries started an uninterrupted charging process as soon as they were plugged into the system.

TABLE II
CASE DESCRIPTION

Case	EV	EV V2G	DG	Forecast error (%)	EV Balance A/B/C	Tesla:Leaf Ratio
Dumb Charge	240	160	x	x	33.25/33.25/33.5	10:0
I;IX	240	160	x	x	33.25/33.25/33.5	10:0
II	240	160	x	x	28/35/37	10:0
III	240	160	✓	x	33.25/33.25/33.5	10:0
IV	400	x	x	x	33.25/33.25/33.5	10:0
V	240	160	x	10	33.25/33.25/33.5	10:0
VI	240	160	x	x	33.25/33.25/33.5	9:1
VII	180	120	x	x	33.25/33.25/33.5	10:0
VIII	120	80	x	x	33.25/33.25/33.5	10:0

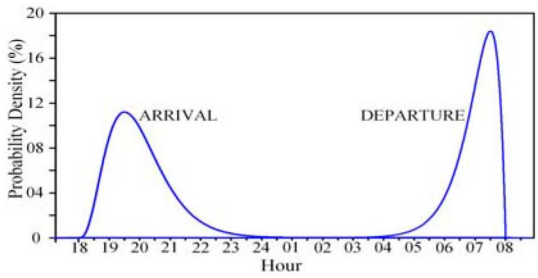

Fig. 3. Arrival and departure distribution function probability.

In Case III, the EDS had two DGs connected at nodes 56 and 104, with energy cost $\alpha^G_{n,t}$ equal to 0.04 US$/kWh. The maximum active powers were 1200 kW and 400 kW, respectively. The minimum and maximum reactive powers were equal to –300 kVAr and 300 kVAr and –100 kVAr and 100 kVAr, respectively. Finally, the minimum power factor for the operation of both DGs was 0.90. As described in section III, the model takes into account the later connection of EVs. In the initial time intervals, the estimated arrivals and initial SOCs of expected EVs are included to avoid overloads in the system. Case V studied a scenario in which 10% of the forecasts for arrivals and initial SOCs were not correct. This test was carried to identify the performance of the proposed methodology when there is unexpected power demand. Cases VII and VIII have been included to demonstrate the performance of the formulation under different levels of EV penetration in the EDS.

For Cases I–VIII, the arrival and departure time intervals were generated based on the two chi-squared probability functions with 8 and 4 degrees of freedom, respectively, as shown in Fig. 3. Moreover, the initial SOC of the EVs was generated using the normal-based probability function displayed in Fig. 4. The mean value and the standard deviation of the SOC probability function were set at 15 and 10, respectively. All of the values were maintained within the red limits shown in both figures. The model was implemented in AMPL [28] and solved with CPLEX [29] using a computer with an Intel $i7$ 4770 processor. The time limit for the solution process in each time interval was 180s.

Table III shows a summary of the results from the test cases. For all of the tests, the resultant EV charging schedule presented no energy curtailment, which means that all of the EVs were completely charged at the time of departure. In Figs. Fig. 5–Fig. 17, the power related to the grid and EV-battery energy

TABLE III
SUMMARY OF THE TEST CASES

Case	Objective Function (US$)	Total E_u^{SH} (kWh)	Energy from V2G (kWh)	Number of Used EV-V2Gs	Energy from DG (kWh)
Dumb Charge	2564.81	0	0	0	0
I	1921.85	0	1825	124	0
II	1921.92	0	1825	124	0
III	1606.50	0	1837.5	128	11200
IV	1996.47	0	0	0	0
V	1921.33	0	1840	128	0
VI	1903.69	0	1716.5	128	0
VII	1846.40	0	1360	96	0
VIII	1765.92	0	990	68	0
IX	2037.75	0	977.5	105	0

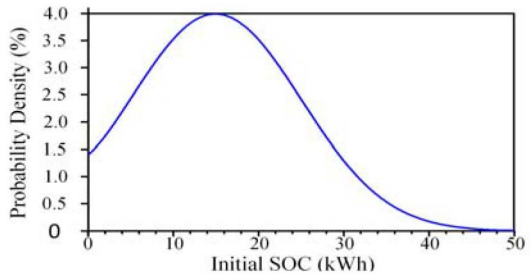

Fig. 4. Initial SOC distribution function probability.

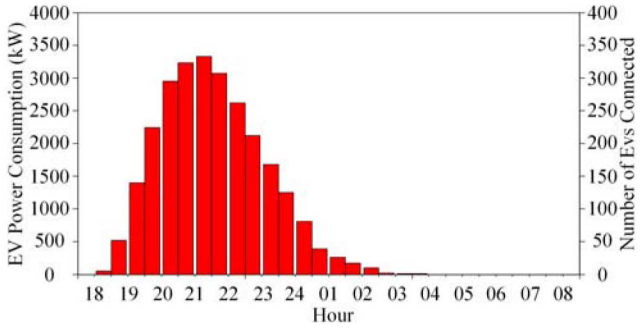

Fig. 5. Dumb Charge simulation results.

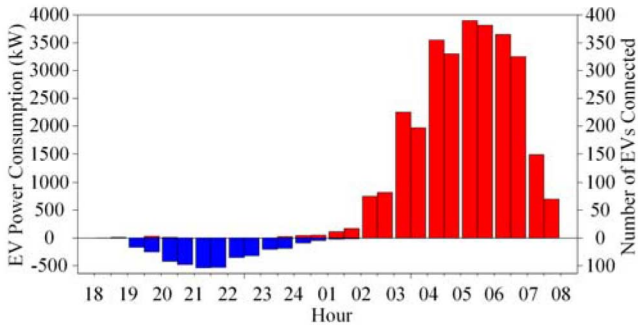

Fig. 6. Case I simulation results.

exchange are shown for each case. The power related to the charging of EVs is shown in red, while the power related to the discharging of EV-V2Gs is shown in blue. Following convention, the EV charging power and the EV-V2G discharging power are given in positive and negative values, respectively.

Figure 5 presents the EV power for the Dumb Charge Case. As explained, no coordination was applied to the EV batteries at recharge, and all vehicles were continuously charged upon being plugged into the grid. The peak load for this case was between 21:00 and 22:00, that is, the time when most vehicles had arrived and were already plugged in. As shown in Table III, this case presented the highest objective function due to the

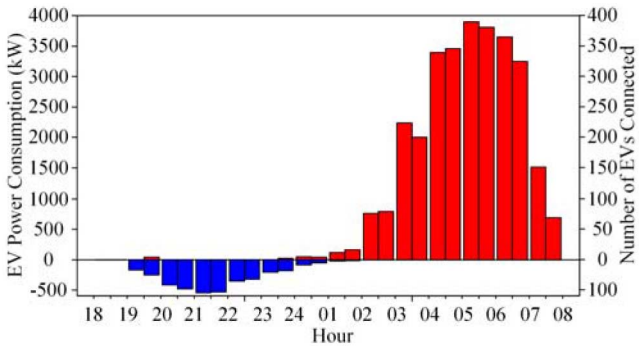

Fig. 7. Case II simulation results.

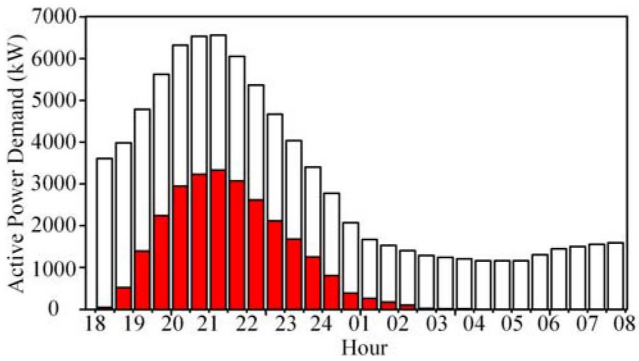

Fig. 8. Dumb Charge total active power demand.

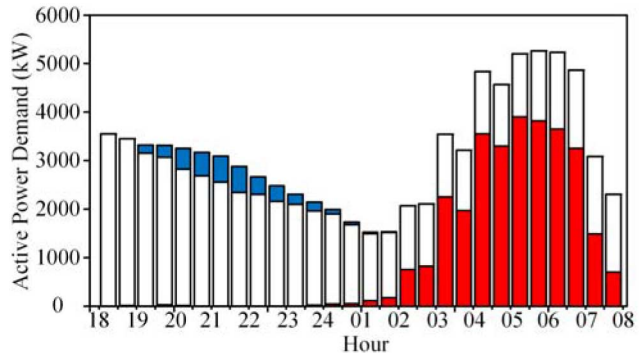

Fig. 9. Case I total active power demand.

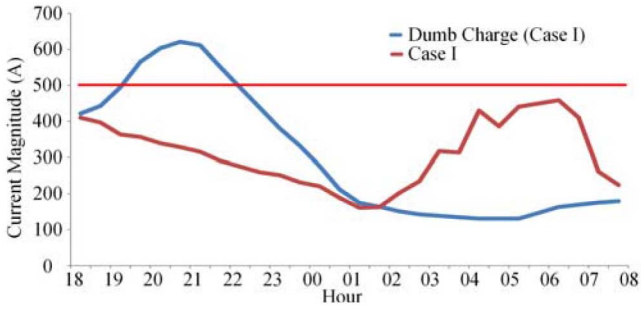

Fig. 10. Maximum current magnitudes (Dumb Charge vs Case I)

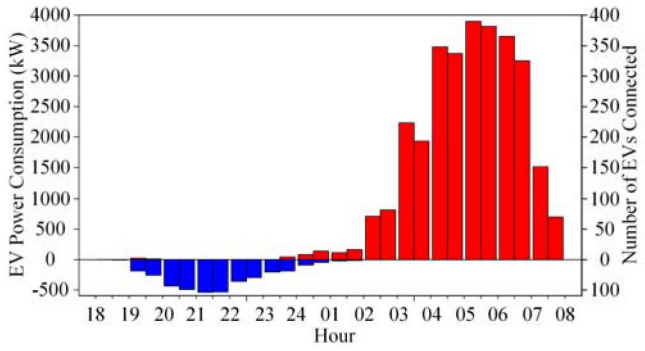

Fig. 11. Case III simulation results.

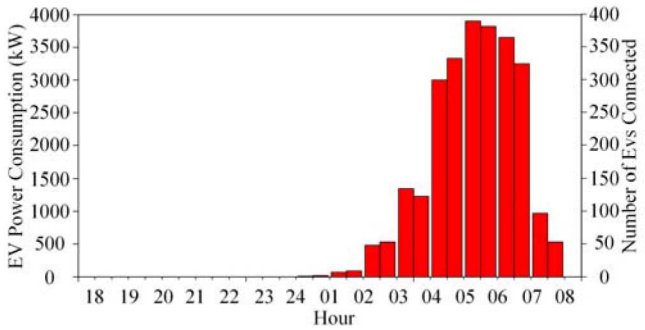

Fig. 12. Case IV simulation results.

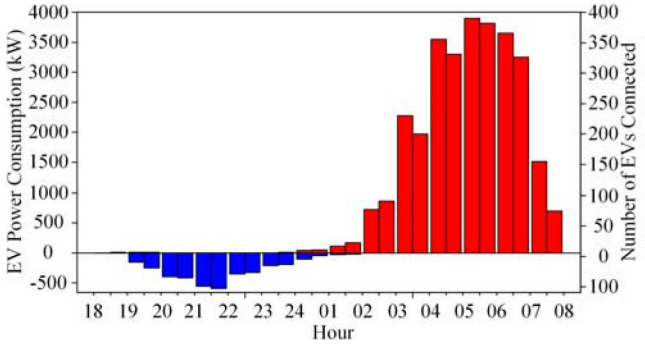

Fig. 13. Case V simulation results.

fact that the EV recharge peak load corresponded with the time intervals when energy prices were the highest.

Figures 6 and 7 show the solutions for Cases I and II. For Case I the EVs were balanced on the EDS phases, while for Case II the EV imbalance shown in Table II was considered. Table III shows a a very small difference between the objective functions of these two cases, evidencing the flexibility of the model when there is an imbalance in the EVs connected.

The total active power demand for the dumb charge case and Case I are shown in Figs. 8 and 9, respectively. As the EVCC is included, the load peak is reduced and reallocated to the low-cost energy time intervals. Figs. 10 and 19 depict the overload on the EDS and the voltage statutory limit outstrip, respectively, due to the uncoordinated connection of EVs. Hence, the coordination of EV recharging in the EDS is beneficial not only for load peak reduction, but also for maintaining the operation of the EDS within the stipulated voltage and thermal limits.

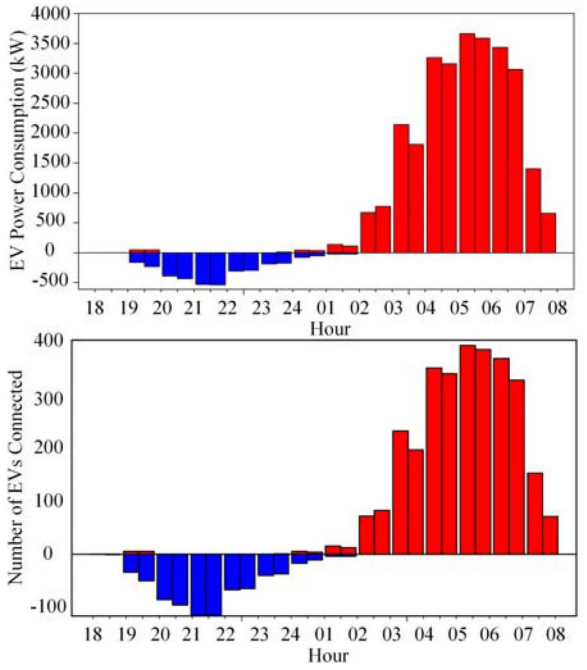

Fig. 14. Case VI simulation results.

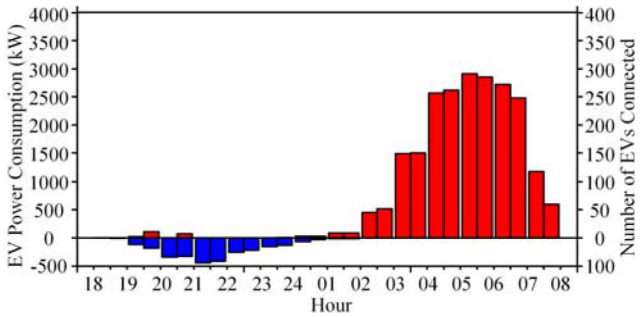

Fig. 15. Case VII simulation results.

The inclusion of DGs was studied in Case III. This case presented the lowest objective function because of the utilization of the low cost energy from the DGs. Due to the alleviation that DGs offer to the EDS, Fig. 11 shows how more EVs were able to be charged during high energy cost time intervals with a substantial reduction to the objective function. Figure 12 shows the power exchange for Case IV, where the V2G technology was disregarded for all vehicles. The objective function for this case rose by 4% when compared to Case I, evidencing the improvement offered by V2G technology. Similar to all the presented cases with controlled EV recharge, the EV peak load of Case IV was between 05:00 and 06:00; yet, in the best charging schedule found for this case, no EVs were charged before midnight.

As shown in Table III, Case V included a 10% forecast error. This means that 10% of the EVs had a mistaken forecast in terms of the time of arrival and initial SOC. In the initial time intervals when most of the EVs have not yet arrived, the methodology finds charging schedules using data from inaccurate forecasts. These schedules may not fit the EVs' actual plugging periods and energy requirements. Unexpected late arrivals and low initial SOCs may create overloads on the EDS

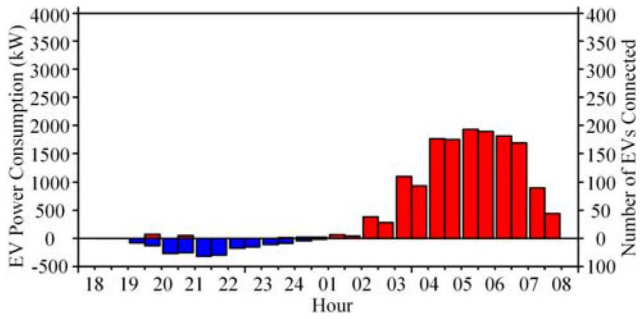

Fig. 16. Case VIII simulation results.

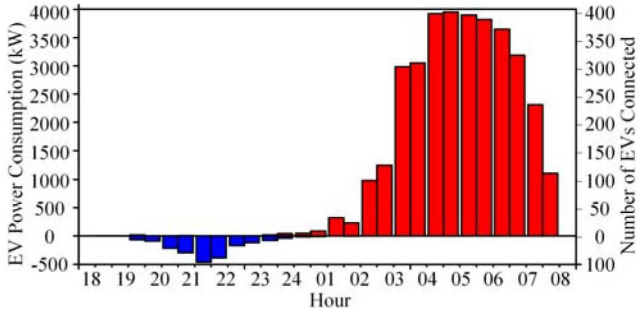

Fig. 17. Case IX simulation results.

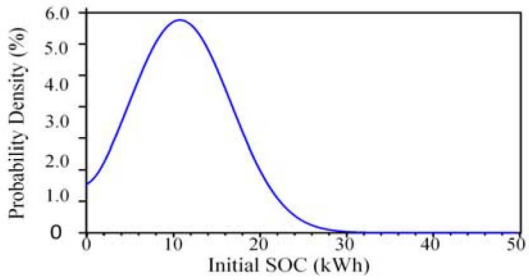

Fig. 18. Initial SOC distribution function probability Case IX.

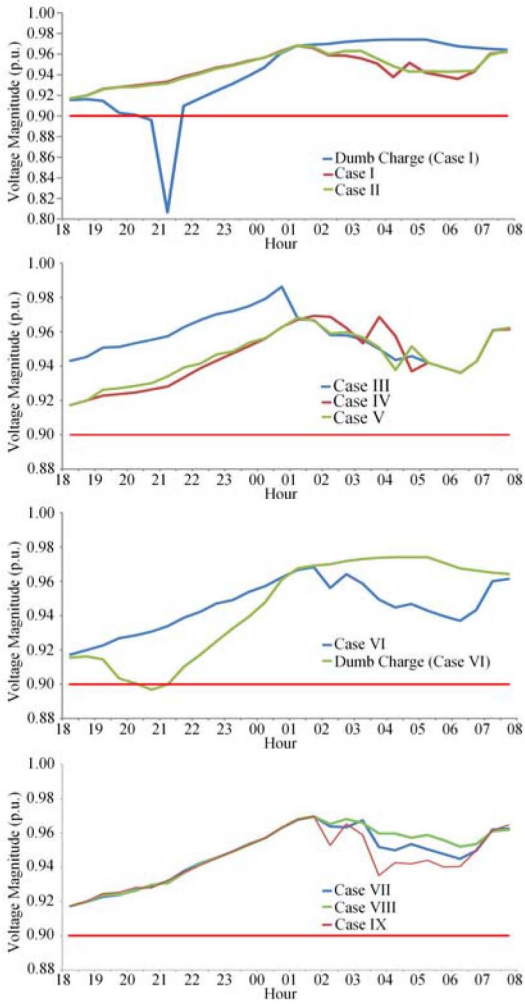

Fig. 19. Minimum voltage magnitudes.

or force energy curtailments on the EV batteries. Even under these conditions, the methodology found a charging schedule with null energy curtailment and with a minimal difference in terms of the objective function. These results demonstrate the adaptability of the methodology when unforeseen changes occur in the EVs' arrivals or SOCs. Case VI tested the proposed method with different types of batteries connected to the grid. 10% of the EVs that were plugged in were Nissan Leafs with the aforementioned specifications. The solution found presented no energy curtailment and a US$603.91 improvement in the objective function compared to uncontrolled EV charging under Case VI conditions; however, the objective function value cannot be compared with previous cases because the EV energy demand of Case VI was less, since smaller batteries were connected to the grid. Furthermore, Cases VII and VIII were tested in order to demonstrate the efficiency of the methodology with different EV penetration. Both charging schedules were developed with no energy curtailment for the EVs.

For Case IX, the values of the initial SOC were obtained by applying the formulation presented in [20] to a mid-sized city in Brazil. Figure 18 shows the probability distribution function obtained from this data. The mean and standard deviation calculated for the sample were 10.78 kWh and 5.90 kWh, respectively. The initial SOC profile obtained was lower than that one used in the previous cases. As expected and as shown in Table III, the energy demand of the complete EV fleet is higher than in Case I, which is directly reflected in an increase in the objective function. For this case, the methodology found a solution that also presents no energy curtailment on the EV batteries.

The minimum voltage in the EDS for each time interval is shown in Fig. 19 for all test cases. For the dumb charge scenario, the EDS did not satisfy operational constraints, as the voltage magnitude dropped below the acceptable limit between 20:00 and 22:00. This fact demonstrate the significance of the burden added to the grid by the EVs and proves the importance of a coordinated EV recharging schedule. For all cases including V2G technology, the EV-V2G energy available for the grid was used during earlier time intervals due to their high energy cost. At the same time, the charging process for most EVs occurred during the final time intervals when the EDS had low energy costs. The charging process was completed between arrival and departure times, and all presented cases generated

schedules ensuring that the EVs left with a fully charged battery at the end of the charging period.

Comparing Case I and Case IV, as shown in Table III, the objective function was reduced by 3.74% when the V2G property of the EVs was considered. At the end of the time period, the economic improvement for the EDS was US$74.62. In Case I, 100% of the EV-V2Gs with energy available and connected to the grid were employed; in more than 98% of the cases, all the available energy was drawn from the EV-V2Gs.

The EV-V2G owners should be compensated for the energy delivered to the grid, as this energy is used during high energy cost time intervals and supplied back during low energy cost time intervals. This compensation corresponds to the additional energy consumed by the EV-V2G to recharge the battery up to its initial value. At the same time, the maximum number of feasible charge cycles of an EV battery is directly influenced by the DoD. Therefore, the lifetime of an EV battery is reduced as the discharge depth is increased for each cycle. The following calculation can be used to estimate the minimum compensation for EV-V2G owners with respect to anticipated EV battery replacement.

As they plug into the system, the average DoD of the EV-V2Gs used by the grid in Case I is 60%; later, once the grid has taken the energy from the V2G function, the average DoD of the EV-V2G reaches 90%. Reference [15] presents a characteristic curve of charge cycles influenced by the DoD of the battery. The number of charge cycles for the EV batteries drops from 4,357 to 2,497. In other words, the expected lifetime of the EV battery is shortened from 12 years (4,357 cycles) to 7 years (2,497 cycles).Therefore, EV-V2G owners must be reimbursed for the deterioration of their EV batteries in order for them to allow their EVs to provide the V2G service.

Assuming a battery replacement cost of US$300 per kWh of storage capacity [30], the 50 kWh Tesla model used in this work will have a battery cost of US$15,000. The annualized value for an EV battery replacement increases from US$2,201.40 for a 12-year lifetime, disabling V2G, to US$3,081.10 for a 7-year lifetime, enabling V2G. Over a 1-year period, the estimated battery replacement cost to be reimbursed to each EV-V2G owner would be US$879.70.

The proposed charging coordination approach can be incorporated into a simple market scheme in which an aggregator synchronizes the charge and discharge operations of multiple EVs, similar to the proposals in [11] and [17]. In such a scheme, EV-V2G owners may be remunerated for different services provided by their vehicles. The aggregator ensures that EVs provide a practical service to the EDS through the utilization of V2G technology. In addition, the aggregator must elaborate and sign bilateral contracts with the EV owners and the EDS. The aggregator receives payments from the EDS due to, among others, V2G energy delivery, energy quality improvements, and avoidance of technical limit violations. On the other hand, the aggregator make payments to the EV owners due to the energy delivered from V2G, battery depreciation, and available power capacity, among others.

Assuming that the benefit obtained from using V2G technology is equally divided among the EV-V2G owners annually, each owner would receive an amount of US$219,65. This amount is 25% of the battery replacement amount due to the utilization of V2G. Hence, it may be assumed that for the simulated case and from an EV owner's point of view, it is not economically appealing to allow the use of the V2G service. Nevertheless, it is important to note, that this only considers the economic enhancement of the EDS operation as related to energy costs. Meanwhile, important features that are highly affected by V2G enabling are disregarded, such as voltage and frequency regulation, voltage and current profile improvements, technical limit violation avoidance and power capacity availability. Considering these features and with the decreasing trend of battery prices, V2G utilization may become appealing to EV owners over the mid-term. In light of this, the presented charging control methodology is increasingly important.

VI. Conclusion

A step-by-step methodology based on a mixed integer linear programming formulation was presented to solve the optimal charging coordination of electrical vehicles (EV) in unbalanced electrical distribution systems (EDS) considering vehicle-to-grid (V2G) technology. The proposed method can be used to define optimal charging schedules in order to avoid operational concerns associated with uncontrolled EV recharging.

The methodology was proven to efficiently handle EV load imbalance; randomness in EVs' arrival and departure times, and initial state of charge; different battery sizes; and forecast uncertainties. For every scenario, the methodology found charging schedules with no EV energy curtailment. In addition, the charging schedules satisfied operational constraints, taking into account the imbalance of the system circuits and loads; they also achieved a better economical operation of the EDS.

These results show the methodology to be very useful, as it defines each step to be implemented and gives a broad view of the state of the EDS throughout the whole time period. The methodology also offers great adaptability for incorporating new loads, e.g. EV plugs for recharge. Also, from the tests carried out, it can be concluded that the utilization of V2G in EDS is economically unsound, because the impact on the battery lifetime outstrips the economical improvement shown by this technology.

Acknowledgement

The authors would like to thank Joel D. Melo and Prof. Antonio Padilha-Feltrin for their support and the data provided.

References

[1] T. Bevis, B. Hacker, C. S. Edrington, and S. Azongha, "A review of PHEV grid impacts," in *Proc. North Amer. Power Symp.*, 2009, pp. 1–6.

[2] N. Anglani, F. Fattori, and G. Muliere, "Electric vehicles penetration and grid impact for local energy models," in *Proc. Energy Conf. Exhib.*, Sep. 9–12, 2012, pp. 1009–1014.

[3] S. Lin, Z. He, T. Zang, and Q. Qian, "Impact of plug-in hybrid electric vehicles on distribution systems," in *Proc. Int. Conf. Power Syst. Technol.*, 2010, pp. 1–5.

[4] W. Di, D. C. Aliprantis, and K. Gkritza, "Electric energy and power consumption by light-duty plug-in electric vehicles," *IEEE Trans. Power Syst.*, vol. 26, no. 2, pp. 738–746, May 2011.

[5] S. Sojoudi and S. H. Low, "Optimal charging of plug-in hybrid electric vehicles in smart grids," in *Proc. IEEE Power Energy Soc. Gen. Meeting (PES)*, 2011, pp. 1–6.
[6] A. Trippe, T. Massier, and T. Hamacher, "Optimized charging of electric vehicles with regard to battery constraints—Case study: Singaporean car park," in *Proc. IEEE Energytech*, May 2013, pp. 1–6.
[7] A. O'Connell, D. Flynn, and A. Keane, "Rolling multi-period optimization to control electric vehicle charging in distribution networks," *IEEE Trans. Power Syst.*, vol. 29, no. 1, pp. 340–348, Jan. 2014.
[8] M. F. Shaaban, M. Ismail, E. F. El-Saadany, and W. Zhuang, "Real-time PEV charging/discharging coordination in smart distribution systems," *IEEE Trans. Smart Grid*, vol. 5, no. 4, pp. 1797–1807, Jul. 2014.
[9] S. Deilami, A. S. Masoum, P. S. Moses, and M. A. S. Masoum, "Real-time coordination of plug-in electric vehicle charging in smart grids to minimize power losses and improve voltage profile," *IEEE Trans. Smart Grid*, vol. 2, no. 3, pp. 456–467, Sep. 2011.
[10] E. L. Karfopoulos and N. D. Hatziargyriou, "A multi-agent system for controlled charging of a large population of electric vehicles," *IEEE Trans. Power Syst.* vol. 28, no. 2, pp. 1196–1204, May 2013.
[11] I. Unda, P. Papadopoulos, S. Skarvelis-Kazakos, L. M. Cipcigan, N. Jenkins, and E. Zabala, "Management of electric vehicle battery charging in distribution networks with multi-agent systems," *Electr. Power Syst. Res.*, vol. 110, pp. 172–179, May 2014.
[12] P. Papadopoulos, N. Jenkins, L. M. Cipcigan, I. Grau, and E. Zabala, "Coordination of the charging of electric vehicles using a multi-agent system," *IEEE Trans. Smart Grid*, vol. 4, no. 4, pp. 1802–1809, Dec. 2013.
[13] A. T. Al-Awami and E. Sortomme, "Coordinating vehicle-to-grid services with energy trading," *IEEE Trans. Smart Grid*, vol. 3, no. 1, pp. 453–462, Mar. 2012.
[14] W. Kempton and J. Tomic, "Vehicle-to-grid power fundamentals: Calculating capacity and net revenue," *J. Power Sour.*, vol. 144, no. 1, pp. 268–279, Jun. 2005.
[15] L. Liu, C. Sohn, G. Balzer, A. Kessler, and F. Teufel, "Economic assessment of lithium-ion batteries in terms of V2G utilisation," in *Proc. Int. Conf. Expo. Elect. Power Eng.*, Oct. 25–27, 2012, pp. 934–938.
[16] J. Van Roy, S. De Breucker, and J. Driesen, "Analysis of the optimal battery sizing for plug-in hybrid and battery electric vehicles on the power consumption and V2G availability," in *Proc. Int. Conf. Intell. Syst. Appl. Power Syst.*, Sep. 25–28, 2011, pp. 1–6.
[17] S. Han, S. Han, and K. Sezaki, "Development of an optimal vehicle-to-grid aggregator for frequency regulation," *IEEE Trans. Smart Grid*, vol. 1, no. 1, pp. 65–72, Jun. 2010.
[18] K. N. Kumar, B. Sivaneasan, P. H. Cheah, P. L. So, and D. Z. W. Wang, "V2G capacity estimation using dynamic EV scheduling," *IEEE Trans. Smart Grid*, vol. 5, no. 2, pp. 1051–1060, Mar. 2014.
[19] H. Yifeng, B. Venkatesh, and L. Guan, "Optimal scheduling for charging and discharging of electric vehicles," *IEEE Trans. Smart Grid*, vol. 3, no. 3, pp. 1095–1105, Sep. 2012.
[20] J. D. Melo, E. M. Carreño, and A. Padilha-Feltrin, "Spatial-temporal simulation to estimate the load demand of battery electric vehicles charging in small residential areas," *J. Control Autom. Elect. Syst.*, vol. 25, pp. 470–480, 2014.
[21] K. Qian, C. Zhou, M. Alan, and Y. Yuan, "Modeling of load demand due to EV battery charging in distribution systems," *IEEE Trans. Power Syst.*, vol. 26, no. 2, pp. 802–810, May 2011.
[22] A. Lojowska, D. Kurowicka, G. Papaefthymiou, and L. Van der Sluis, "Stochastic modeling of power demand due to EVs using copula," *IEEE Trans. Power Syst.*, vol. 27, no. 4, pp. 1960–1968, Nov. 2012.
[23] J. F. Franco, M. J. Rider, and R. Romero, "A mixed-integer linear programming model for the electric vehicle charging coordination problem in unbalanced electrical distribution systems," *IEEE Trans. Smart Grid*, vol. 6, no. 5, pp. 2200–2210, Sep. 2015.
[24] J. F. Franco, M. J. Rider, M. Lavorato, and R. Romero, "A mixed-integer LP model for the reconfiguration of radial electric distribution systems considering distributed generation," *Electr. Power Syst. Res.*, vol. 97, pp. 51–60, Apr. 2013.
[25] Distribution Test Feeders, IEEE/PES. (2014, Oct.). *123-Bus Feeder* [Online]. Available: http://ewh.ieee.org/soc/pes/dsacom/testfeeders
[26] *Tesla Motors Specifications*, Tesla Motors, 2015 [Online]. Available: http://www.teslamotors.com/models/specs
[27] *Nissan Specifications*, Nissan, USA, 2015 [Online]. Available: http://www.nissanusa.com/electric-cars/leaf/
[28] R. Fourer, D. M. Gay, and B. W. Kernighan, *AMPL: A Modeling Language for Mathematical Programming*, 2nd ed. Pacific Grove, CA, USA: Brooks/Cole/Thomson Learning, 2003.
[29] IBM ILOG CPLEX V12.1 User's Manual for CPLEX, CPLEX Division, ILOG Inc., Incline Village, NV, USA, 2009.
[30] B. Nykvist and M. Nilsson, "Rapidly falling costs of battery packs for electric vehicles," *Nat. Clim. Change*, vol. 5, no. 4, pp. 329–332, Mar. 2015.

Carlos Sabillón Antúnez received the B.Sc. degree in electrical engineering from the UNAH, Tegucigalpa, Honduras, the M.Sc. degree in electrical engineering from São Paulo State University (UNESP), Ilha Solteira, Brazil, in 2011 and 2014, respectively. He is currently pursuing the Ph.D. degree in electrical engineering at UNESP. His research interests include development of methodologies for the optimization, planning, and control of electrical power systems.

John F. Franco (S'11–M'13) received the B.Sc. and M.Sc. degrees in electrical engineering from the Universidad Tecnologica de Pereira, Pereira, Colombia, and the Ph.D. degree in electrical engineering from São Paulo State University (UNESP), Ilha Solteira, Brazil, in 2004, 2006, and 2012, respectively. His research interests include development of methodologies for the optimization, planning, and control of electrical power systems.

Marcos J. Rider (S'97–M'06) received the B.Sc. (Hons.) and P.E. degrees from the National University of Engineering, Lima, Peru, the M.Sc. degree from the Federal University of Maranhão, Maranhão, Brazil, and the Ph.D. degree from the University of Campinas (UNICAMP), Campinas, Brazil, all in electrical engineering, in 1999, 2000, 2002, and 2006, respectively. Currently, he is a Professor of Systems and Energy with UNICAMP. His research interests include the development of methodologies for the optimization, planning, and control of electrical power systems, and applications of artificial intelligence in power systems.

Ruben Romero (SM'08) received the B.Sc. and P.E. degrees from the National University of Engineering, Lima, Peru, and the M.Sc. and Ph.D. degrees from the Universidade Estadual de Campinas, Campinas, Brazil, in 1978, 1984, 1990, and 1993, respectively. Currently, he is a Professor of Electrical Engineering with the Universidade Estadual Paulista Julio de Mesquita Filho, Ilha Solteira, Brazil. His research interests include methodologies for the optimization, planning, and control of electrical power systems, applications of artificial intelligence in power system, and operations research.